– Supplementary Information –

Optoelectronic Property Comparison for Isostructural $Cu_2BaGeSe_4$ and Cu_2BaSnS_4 Solar Absorbers

Yongshin Kim,[a] Hannes Hempel,[b] Sergiu Levcenco,[b] Julie Euvrard,[a] Eric Bergmann,[c] Oki Gunawan,[d] Thomas Unold,[b] Ian G Hill,[c] David B. Mitzi*[a,e]

[a]*Department of Mechanical Engineering and Materials Science, Duke University, Durham, North Carolina 27708, USA.*

[b]*Department Structure and Dynamics of Energy Materials, Helmholtz-Zentrum Berlin für Materialien und Energie GmbH, Hahn-Meitner-Platz 1, 14109, Berlin, Germany*

[c]*Department of Physics, Dalhousie University, 6310 Coburg Road, Halifax, Nova Scotia, B3H 4R2, Canada.*

[d]*IBM T. J. Watson Research Center, Yorktown Heights, New York 10598, USA*

[e]*Department of Chemistry, Duke University, Durham, North Carolina 27708, USA.*

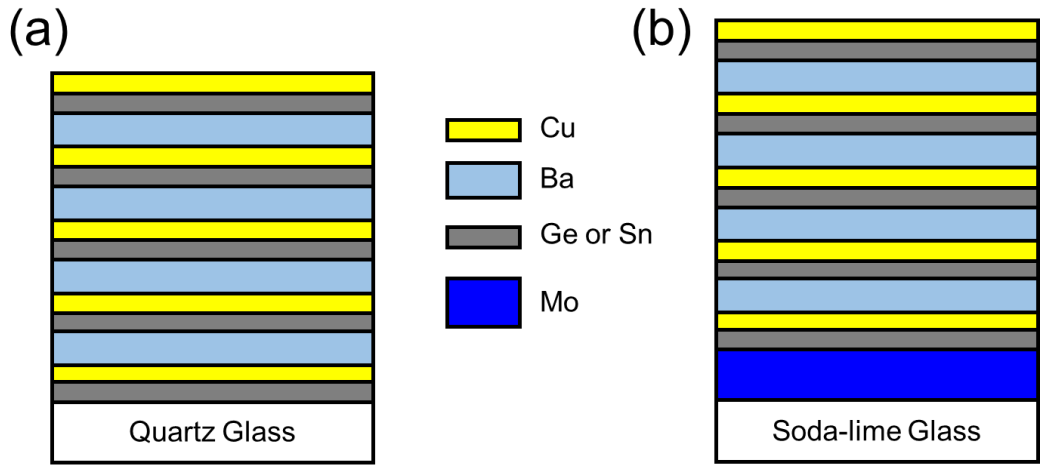

Fig. S1 Precursor configuration for CBGSe (or CBTS) films on (a) quartz glass and (b) Mo-coated soda-lime glass substrates.

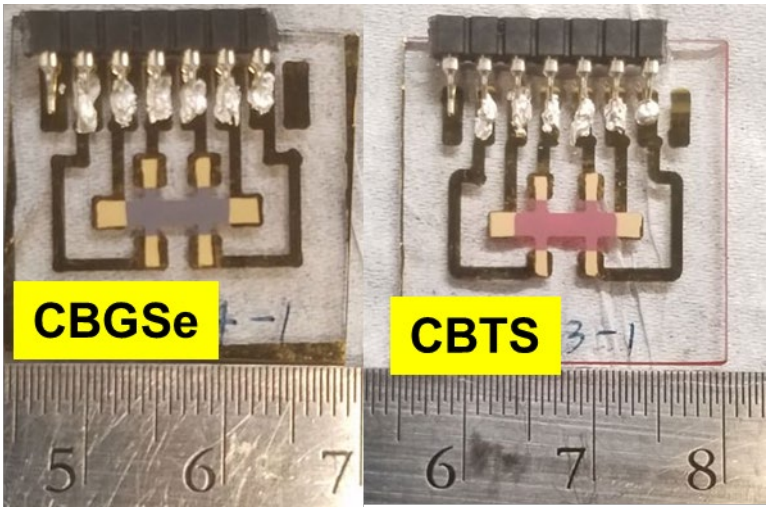

Fig. S2 Image of CBGSe and CBTS devices for Hall measurements.

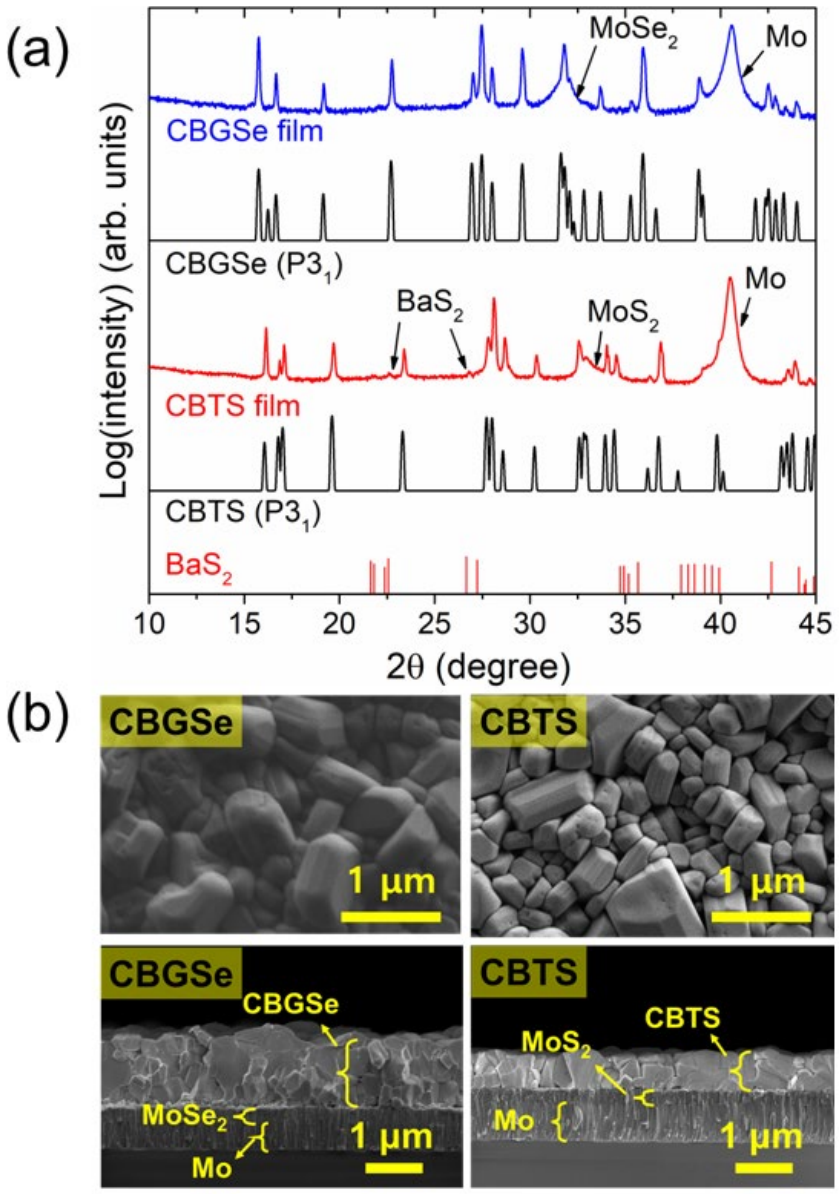

Fig. S3 (a) XRD patterns of CBGSe (blue curve) and CBTS (red curve) films deposited on Mo-coated soda-lime glass substrates. The XRD patterns are compared with simulated XRD patterns (black line) using CrystalDiffract software with lattice parameters adapted from ICDD reference code 01-71-2889 for CBGSe and 03-65-7569 for CBTS. Red stick bars indicate XRD pattern of BaS_2 (ICDD 01-082-1710). (b) Surface and cross-section SEM images of the films.

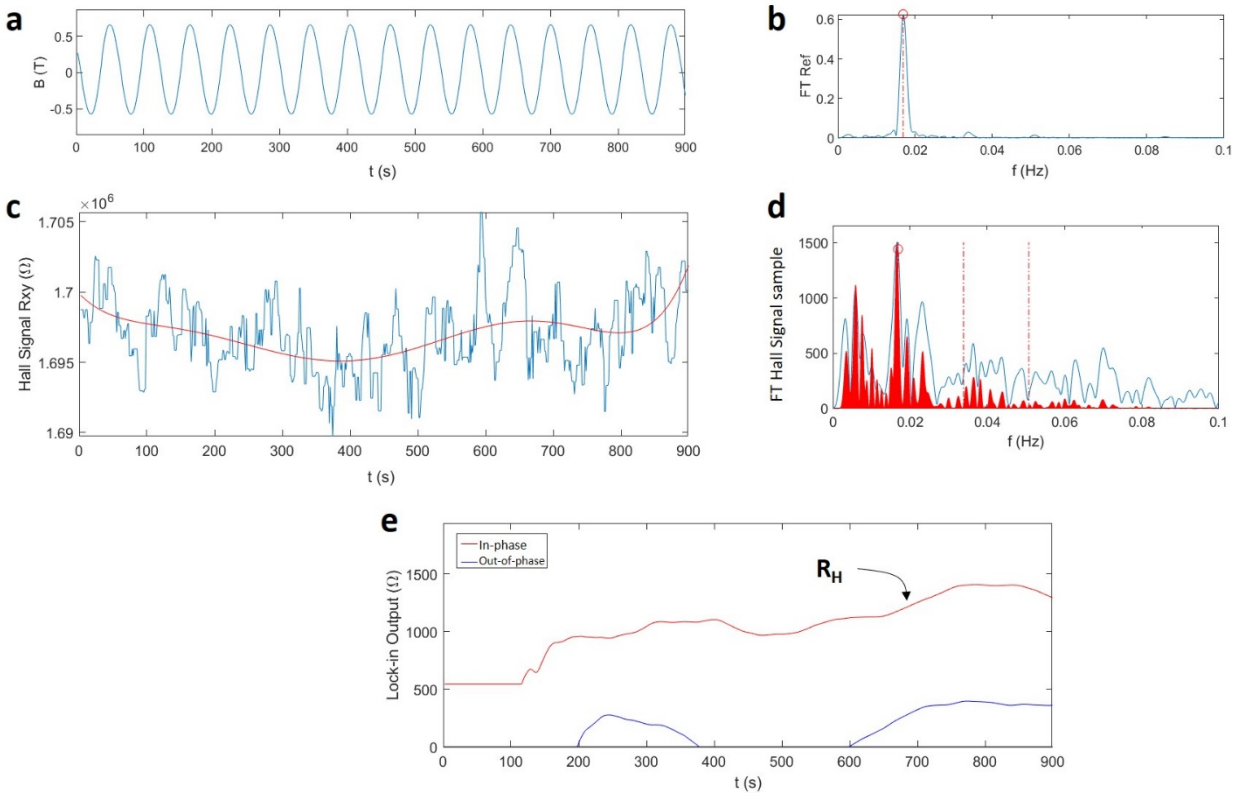

Fig. S4 Hall signal extraction on CBGSe sample using a parallel dipole line (PDL) setup: (a) Magnetic field B traces as the reference signal, and (b) Fourier transform of the reference signal B. (c) Transverse Hall signal R_{XY} and (d) Fourier transform of R_{XY}. The dashed dotted lines correspond to the second and third harmonics of the AC signal B. The red-filled region is the power spectral density (PSD) and the curve is the Fourier spectra of the signal. (e) Lock-in detection of the in-phase (Hall signal) and out-of-phase signals over time where the Hall resistance R_H is extracted. A lock-in time constant of 120s is used in this example.

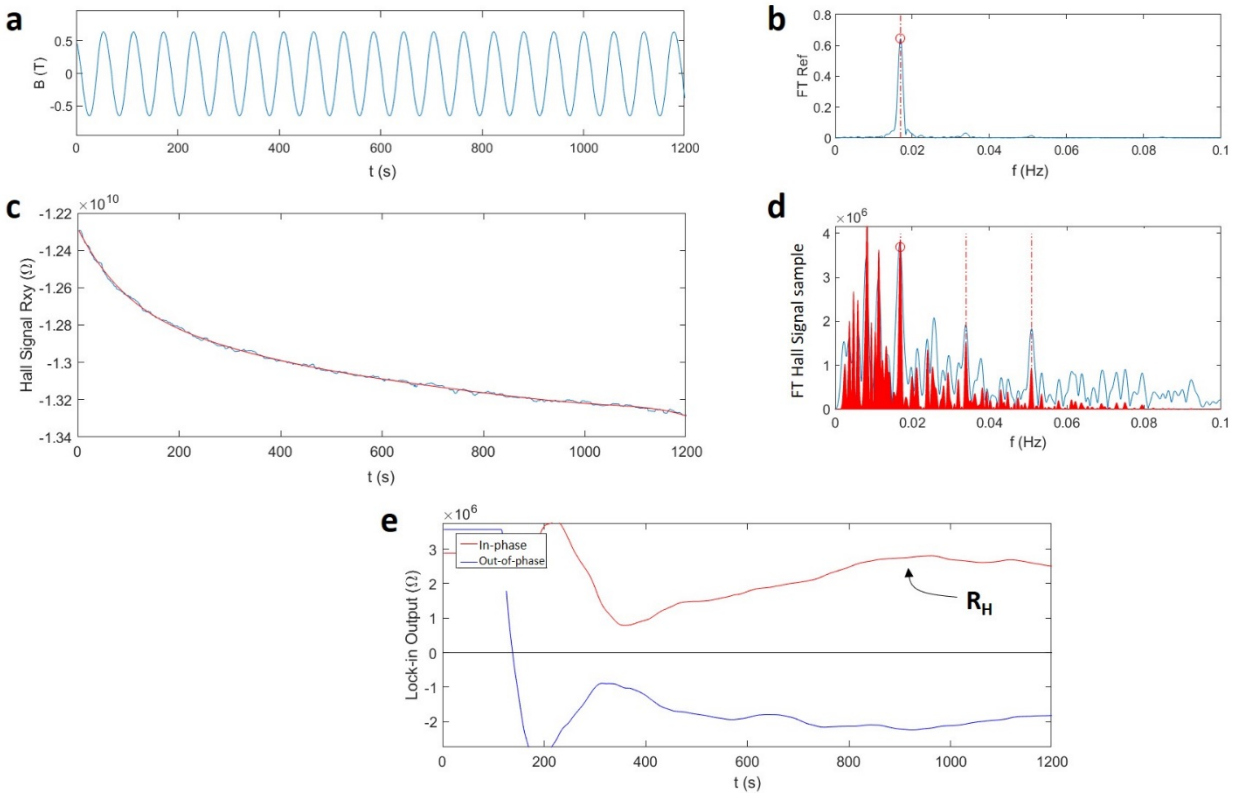

Fig. S5 Hall signal extraction on CBTS sample using a PDL setup: (a) Magnetic field B traces as the reference signal, and (b) Fourier transform of the reference signal B. (c) Transverse Hall signal R_{XY} and (d) Fourier transform of R_{XY}. The dashed dotted lines correspond to the second and third harmonics of the AC signal B. The red-filled region is the power spectral density (PSD) and the curve is the Fourier spectra of the signal. (e) Lock-in detection of the in-phase (Hall signal) and out-of-phase signals over time where the Hall resistance R_H is extracted. A lock-in time constant of 120s is used in this example.

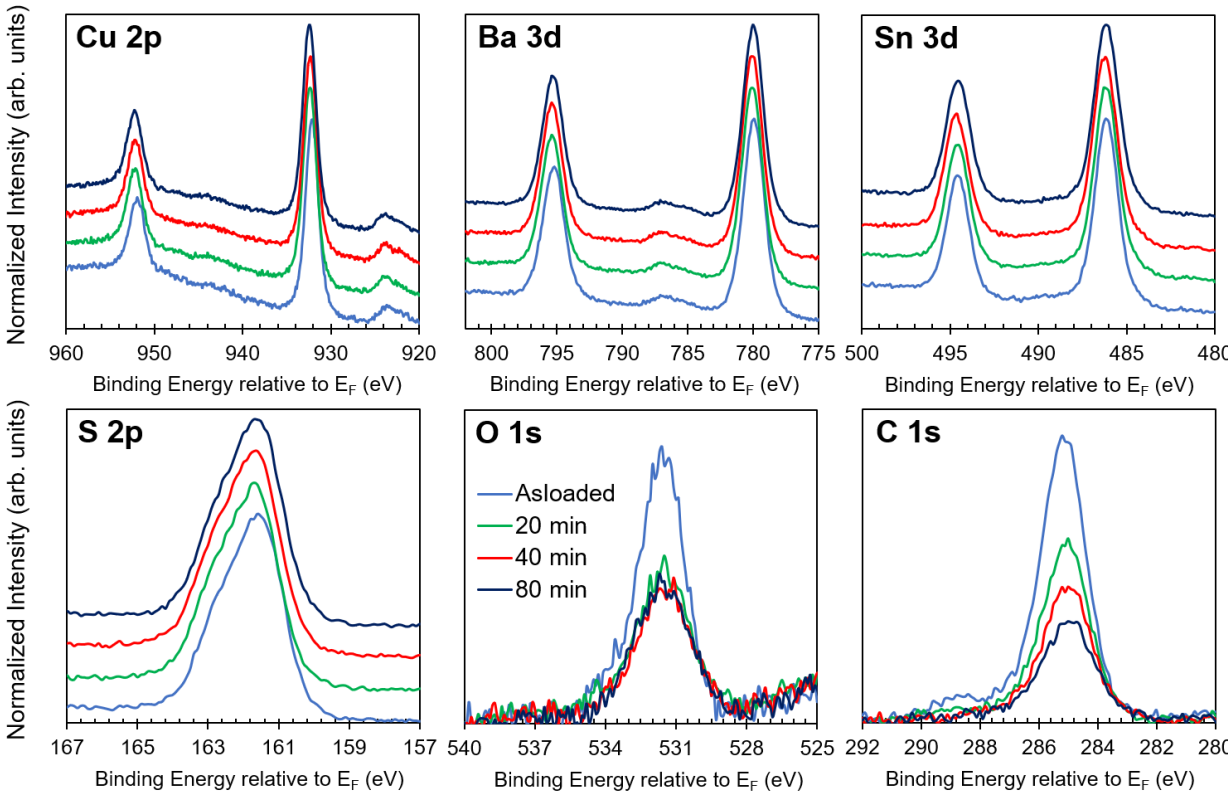

Fig. S6 Al Kα XPS core level spectra of each detected element for the CBTS surface as a function of sputtering time. Spectra for expected Cu 2p, Ba 3d, Sn 3d and S 2p core levels are shifted vertically for clarity to show that their shape and peak broadness are unchanged with sputtering. There is a slight shift (0.1 eV) across all core levels, suggesting mild sputtering induced band bending. Surface contaminant oxygen and carbon core levels are also shown to decrease with sputtering.

Table S1 Atomic abundances and associated uncertainty for each expected element in CBTS films as a function of sputter cleaning time, calculated by fitting XPS core level spectra.

Element (Core level)	Expected abundance	Uncertainty	As-loaded	20 min	40 min	80 min
Cu (2p)	0.250	± 0.004	0.106	0.121	0.132	0.146
Ba (3d)	0.125	± 0.006	0.130	0.131	0.133	0.139
Sn (3d)	0.125	± 0.004	0.126	0.129	0.130	0.128
S (2p)	0.500	± 0.005	0.639	0.619	0.605	0.587

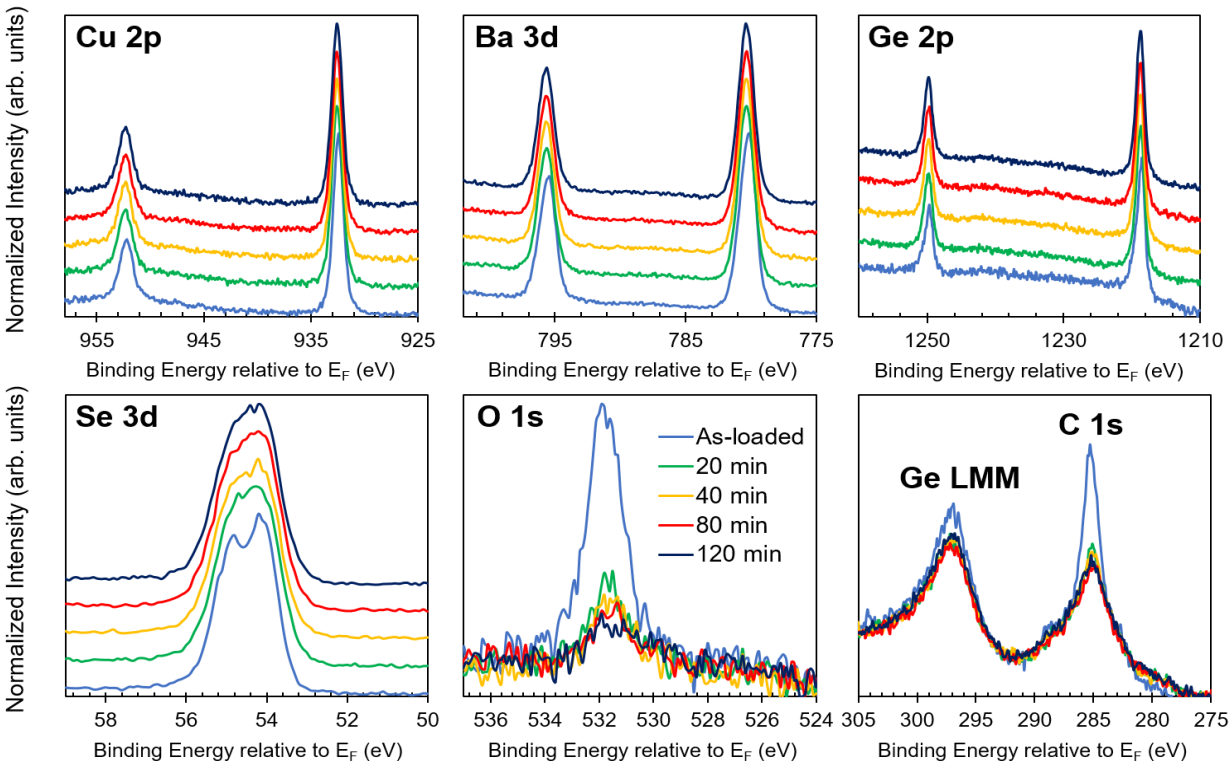

Fig. S7 Al Kα XPS core level spectra of each detected element for the CBGSe surface as a function of sputter time. Spectra for expected Cu 2p, Ba 3d, Ge 2p and Se 3d core levels are vertically shifted for clarity to show that their shape and peak broadness are unchanged with sputtering. There is a slight shift (0.1 eV) across all core levels, suggesting mild sputtering induced band bending. Surface contaminant oxygen and carbon core levels are also shown to decrease with sputtering. Note that the C 1s core level heavily overlaps with two germanium Auger peaks.

Table S2 Atomic abundances and associated uncertainty for each expected element in CBGSe films as a function of sputter cleaning time, calculated by fitting XPS core level spectra.

Element (Core level)	Expected abundance	Uncertainty	As-loaded	20 min	40 min	80 min	120 min
Cu (2p)	0.250	± 0.003	0.172	0.165	0.161	0.162	0.155
Ba (3d)	0.125	± 0.004	0.199	0.200	0.200	0.200	0.202
Ge (2p)	0.125	± 0.006	0.130	0.135	0.136	0.146	0.150
Se (3d)	0.500	± 0.006	0.500	0.501	0.503	0.492	0.493

Table S3 Parameters derived from UPS and IPES measurements for as-loaded and sputtered CBGSe and CBTS surfaces; E_{VBM}, E_{CBM}, E_{onset} energy values are referenced to the Fermi-level.

Sputter duration	CBGSe					CBTS				
	E_{VBM} (± 0.05eV)	E_{CBM} (± 0.2eV)	E_{onset} (± 0.01eV)	EA (± 0.2eV)	E_g (± 0.2eV)	E_{VBM} (± 0.03eV)	E_{CBM} (± 0.2eV)	E_{onset} (± 0.01eV)	EA (± 0.2eV)	E_g (± 0.2eV)
As-loaded	0.60	-1.00	17.16	3.06	1.60	0.55	-1.80	17.17	2.25	2.35
20 min	0.70	-1.10	16.67	3.45	1.80	0.70	-1.30	16.98	2.94	2.00
40 min	0.80	-1.10	16.56	3.56	1.90	0.70	-1.30	16.62	3.30	2.00
80 min	0.80	-1.10	16.45	3.67	1.90	0.70	-1.30	16.64	3.28	2.00
120 min	0.80	-1.10	16.40	3.72	1.90					

Supporting note S1: Eliott model

The Elliot model describes the absorption onset of a direct band gap semiconductor with an exciton (and its excited states) and the continuum contribution, $\alpha = \alpha_x + \alpha_c$: [1-3]

$$\alpha_x \propto \frac{\alpha_0}{E}\left\{\sum_{n=1}^{\infty}\frac{2E_x}{n^3}sech\left[\frac{E - E_g + \frac{E_x}{n^2}}{\Gamma}\right]\right\}$$

$$\alpha_c \propto \frac{\alpha_0}{E}\left\{\int_{E_g}^{\infty}\frac{\text{sech}\,[(E - E')/\Gamma]}{1 - exp\left[-2\pi\sqrt{E_x/(E' - E_g)}\right]}dE\right\}$$

The absorption coefficient of CBTS is modeled by the sum of continuum and exciton contributions, which are convoluted with a broadening parameter of $\Gamma = 24$ meV. Here, E_x is the exciton binding energy, n refers to the principal quantum number, E_g is the band gap, and α_0 is the band-band transition absorption strength in the absence of Coulomb interaction.

The absorption coefficient of CBGSe is modeled by the sum of two continuum contributions and two exciton contributions with an equal exciton binding energy $E_x = 20$ meV and $\Gamma_1 = 19$ meV and $\Gamma_2 = 33$ meV.

Supporting note S2: Fraction of free carriers

Excitons and dissociated electrons and holes coexist in a semiconductor. The fraction of free carriers Δn to total injected carriers, $\phi = \frac{\Delta n}{\Delta n + \Delta n_x}$, where Δn_x is the concentration of excitons, can be estimated from a modified Saha equation, which includes carrier screening and the Mott transition (Ref 4, equation 13).

Fig. S8 shows the quantum yield as a function of total carrier density for the exciton binding energies of 20 meV and 25 meV, which were deduced from modeling the absorption onset. Average relative electron- and hole effective masses of 0.22 and 0.64 for CBTS and 0.16 and 0.41 for CBGSe were used, respectively.[5]

Assuming a best-case minority carrier lifetime of 1 μs, a 1-micron-thick sample and a photon flux of 10^{17} $cm^{-2}s^{-1}$, a steady-state carrier density of ~ 10^{15} cm^{-3} would be estimated under AM1.5 excitation conditions. **Fig. S8** clearly shows that, for this case and all smaller carrier lifetimes, a free carrier quantum yield of close to unity is expected.

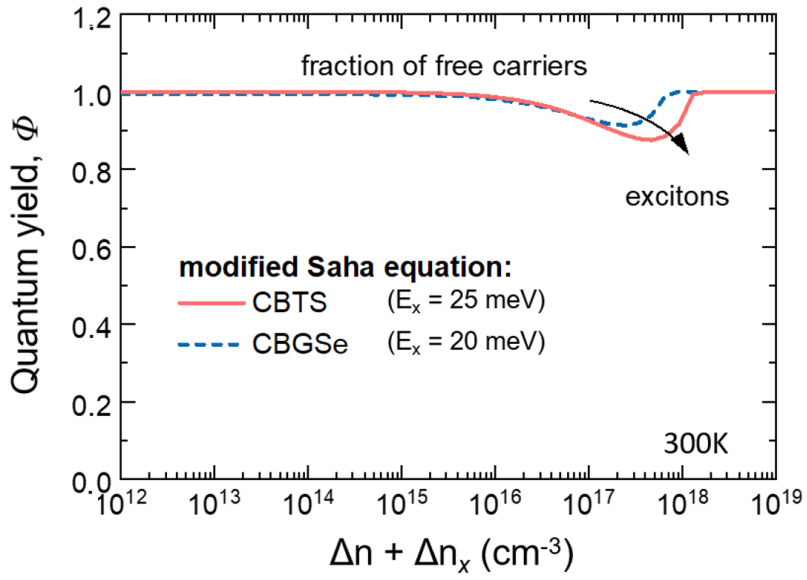

Fig. S8 Fraction of free carriers, or free carrier quantum yield (ϕ), for different exciton binding energies and as a function of total carrier density, $\Delta n+\Delta n_x$, as modeled by the modified Saha equation at 300 K.

From optical-pump terahertz-probe spectroscopy (OPTP), the sum of electron and hole mobilities is obtained by modeling with the well-known Drude formula,

$$\mu_\Sigma = \mu_\mathrm{e} + \mu_\mathrm{h} = \frac{e\tau_{scat}}{m_r}\frac{1}{1 - i\omega\tau_{scat}}$$

$$\frac{1}{m_r} = \frac{1}{m_e} + \frac{1}{m_h}$$

with scattering time τ_{scat} and the reduced mass m_r.[6]

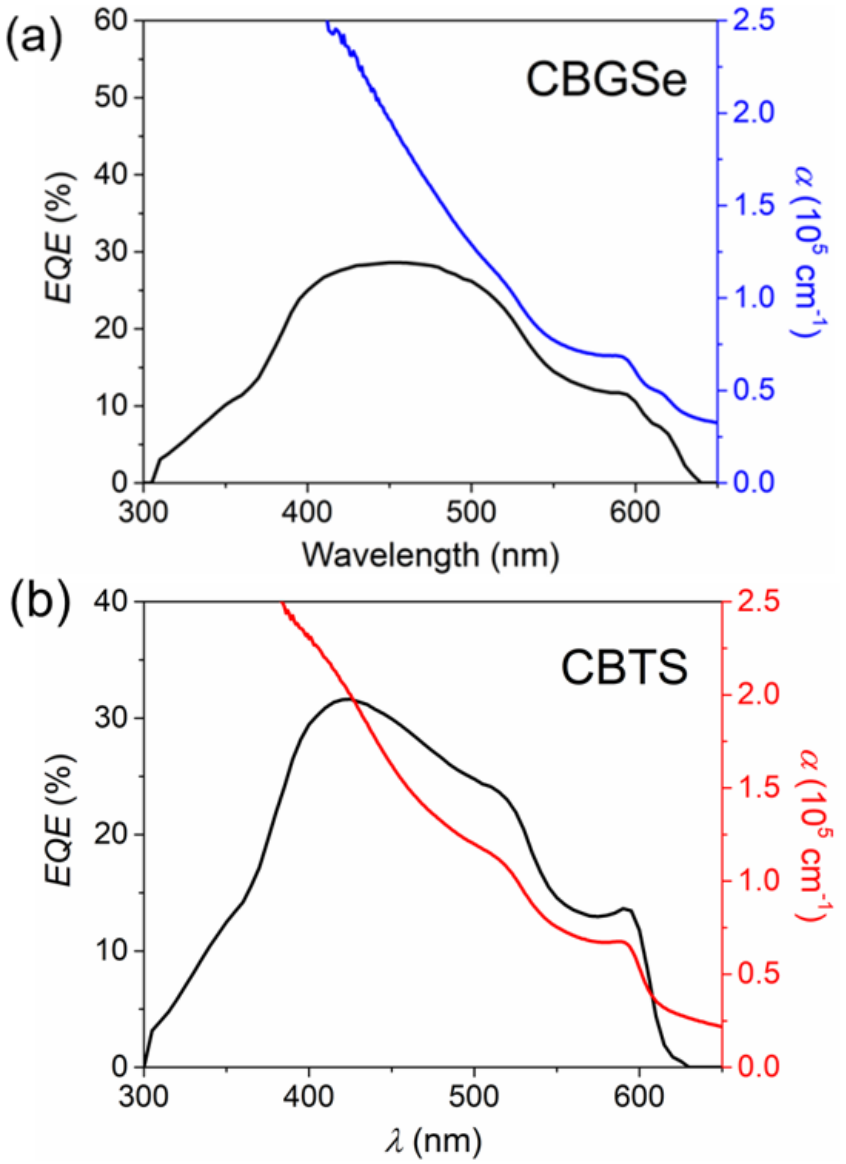

Fig. S9 *EQE* of representative (a) CBGSe and (b) CBTS solar cells along with optical absorption spectra of CBGSe and CBTS films.

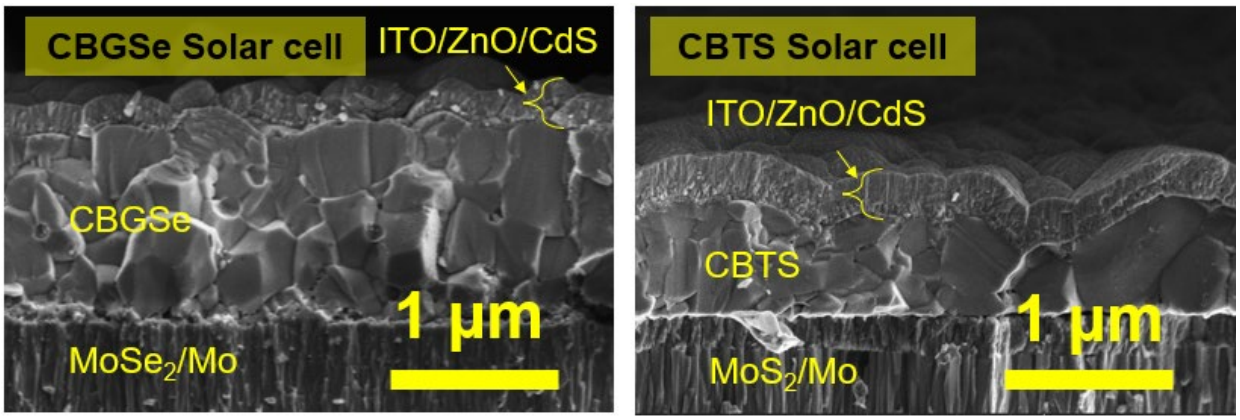

Fig. S10 Cross-section SEM images of representative CBGSe and CBTS solar cells.

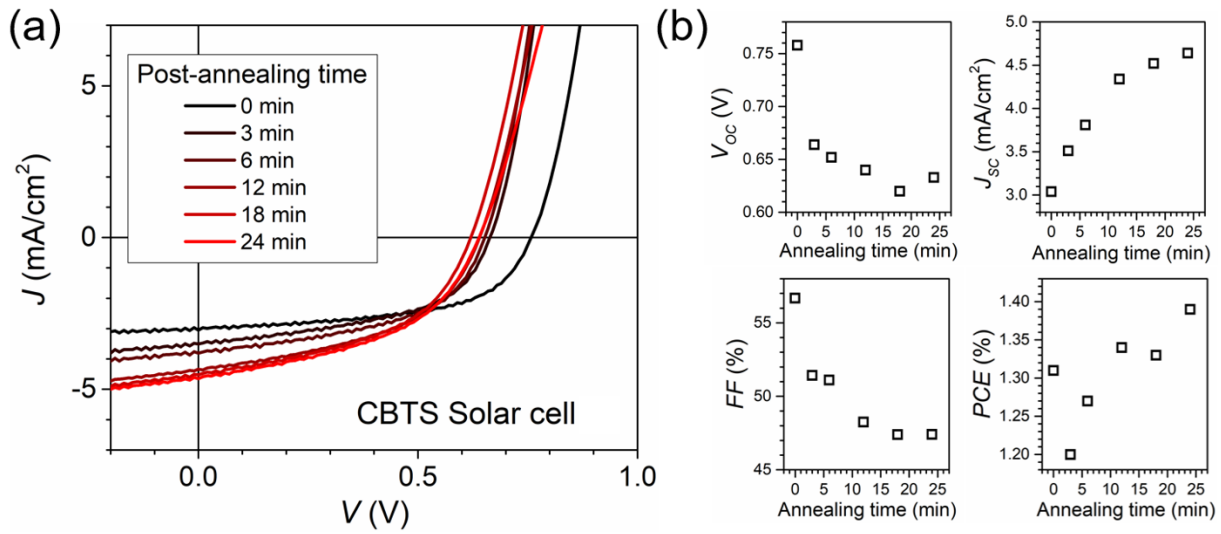

Fig. S11 (a) Impact of post-annealing (at 200°C under ambient air) on the *J-V* curve for a representative CBTS solar cell. (b) Evolution of the solar cell performance parameters with increasing post-annealing time .

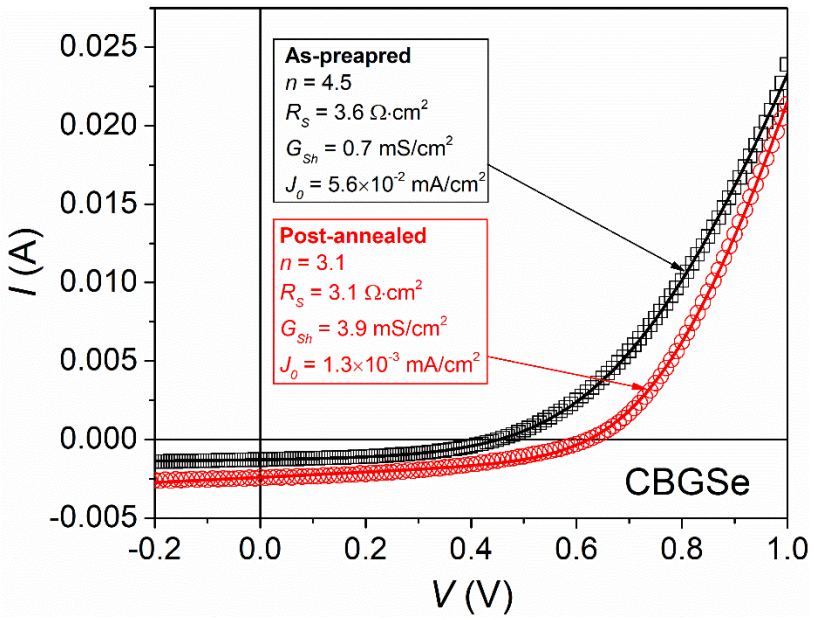

Fig. S12 One-diode model fit of light *I-V* curves of a representative CBGSe solar cell (before and after post-annealing treatment at 200°C for 20 min under ambient air) using Lambert-W fitting method.[7] (The device area is 0.425 cm^2.)

References

1. N. K. Kumawat, A. Dey, A. Kumar, S. P. Gopinathan, K. Narasimhan and D. Kabra, *ACS Appl. Mater. Interfaces,* 2015, **7**, 13119-13124.
2. R. Elliott, *Phys. Rev.*, 1957, **108**, 1384.
3. M. Saba, M. Cadelano, D. Marongiu, F. Chen, V. Sarritzu, N. Sestu, C. Figus, M. Aresti, R. Piras and A. G. Lehmann, *Nature Commun.*, 2014, **5**, 1-10.
4. D. Snoke, *Solid State Commun.*, 2008, **146**, 73-77.
5. T. Zhu, W. P. Huhn, G. C. Wessler, D. Shin, B. Saparov, D. B. Mitzi and V. Blum, *Chem. Mater.*, 2017, **29**, 7868-7879.
6. H. Němec, P. Kužel and V. Sundström, *J. Photochem. Photobiology A: Chem.,* 2010, **215**, 123-139.
7. C. Zhang, J. Zhang, Y. Hao, Z. Lin and C. Zhu, *J. Appl. Phys.*, 2011, **110**, 064504.